Journal of Applied Physics

Ferrofluid-lubricated thrust bearing with an air cushion

Cite as: J. Appl. Phys. **130**, 123902 (2021); https://doi.org/10.1063/5.0064604
Submitted: 25 July 2021 • Accepted: 04 September 2021 • Published Online: 23 September 2021

Xingfei Xie, Qingwen Dai, Wei Huang, et al.

Journal of Applied Physics ARTICLE scitation.org/journal/jap

Ferrofluid-lubricated thrust bearing with an air cushion

Cite as: J. Appl. Phys. **130**, 123902 (2021); doi: 10.1063/5.0064604
Submitted: 25 July 2021 · Accepted: 4 September 2021 ·
Published Online: 23 September 2021

Xingfei Xie, Qingwen Dai, Wei Huang,[a] and Xiaolei Wang

AFFILIATIONS

National Key Laboratory of Science and Technology on Helicopter Transmission, Nanjing University of Aeronautics & Astronautics, Nanjing 210016, China

[a]**Author to whom correspondence should be addressed:** huangwei@nuaa.edu.cn. **Tel./Fax:** +86 25 84893599

ABSTRACT

This study develops a ferrofluid-lubricated thrust bearing with an air cushion. The bearing comprises a rotor, a stator, and a ferrofluid ring formed between them due to absorption by an annular magnet under the stator. The design makes it possible for the air cushion (air sealed inside the ferrofluid ring) as well as the magnetized ferrofluid to supply supporting forces. A model of the bearing for a static supporting force is proposed and validated by experiments. As the gap between the rotor and stator was 0.25 mm, the maximum static supporting force of the bearing was 3.2 N, much higher than the support provided by the pure ferrofluid ring (without the air cushion, 1.7 N). The operating space of the bearing was detected by multicycle load–retract tests with remarkably high and repeatable accuracy. The results of dynamic experiments show that the speed of rotation of the rotor has a minor effect on the supporting force. Such a ferrofluid-lubricated bearing offers promise for use in precise positioning or low-friction systems.

I. INTRODUCTION

Friction is unfavorable in most operating conditions, especially in micro-precision systems. Liquid lubrication is an important means of reducing friction. Traditional hydrostatic[1] and hydrodynamic lubrication[2] can be regarded as representative lubricants due to the bearing capacity of a pressurized liquid.

Liquid bridge bearings have recently been developed as a new model of lubrication.[3–5] The key technology in such bearing is the use of the free energy barrier between hydrophilic and hydrophobic surfaces to restrict the volume of liquid on the hydrophilic surface.[6] Thus, the Laplace pressure built inside the liquid acts as a supporting mechanism and solid–solid contact can be eliminated.[7] The supporting capacity of the bearing usually depends on the volume of liquid and its contact angles on the hydrophilic and hydrophobic surfaces.[8] The liquid bridge bearing has many applications, especially in micro-electromechanical systems (MEMS), because it can support both static and dynamic loads, and is self-centering and wear free.

However, the liquid bridge bearing is not perfect. The supporting force generated by it is small in magnitude, usually of the order of 10^{-1} N.[9] As the contact angle of the liquid on a superhydrophobic surface attains the value of its advancing contact angle, droplets escape from the liquid bridge[9] to reduce the volume of liquid as well as the supporting force provided by it. In addition, to attain the surface energy barrier, patterned surfaces with an alternant hydrophobic/hydrophilic structure should be pre-fabricated on the surface of the substrate. Questions then arise: Can the liquid be positioned by other types of energy barriers? Excluding the surface tension dominated by Laplace pressure, can the lifting force be further increased by any other support mechanism?

The ferrofluid (FF) is a colloidal suspension in which magnetic particles are uniformly dispersed in a carrier liquid.[10] To avoid coagulation, the surfaces of these particles are coated with a surfactant. The mean diameter of each particle is about 10 nm.[11] Given this size, each nanoparticle may be treated as a tiny permanent magnet.[10] From the fluid mechanical point of view, the FF is interesting because it can always be located in the desired position in the presence of an external magnetic field,[12] and the randomly oriented poles of each particle may align along the direction of the external field. From the physical point of view, the FF is interesting due to mechanisms of the transformation of the magnetostatic repulsive force formed on each particle into a magnetic body force in the fluid or an additional "magnetic pressure."[13] Compared with

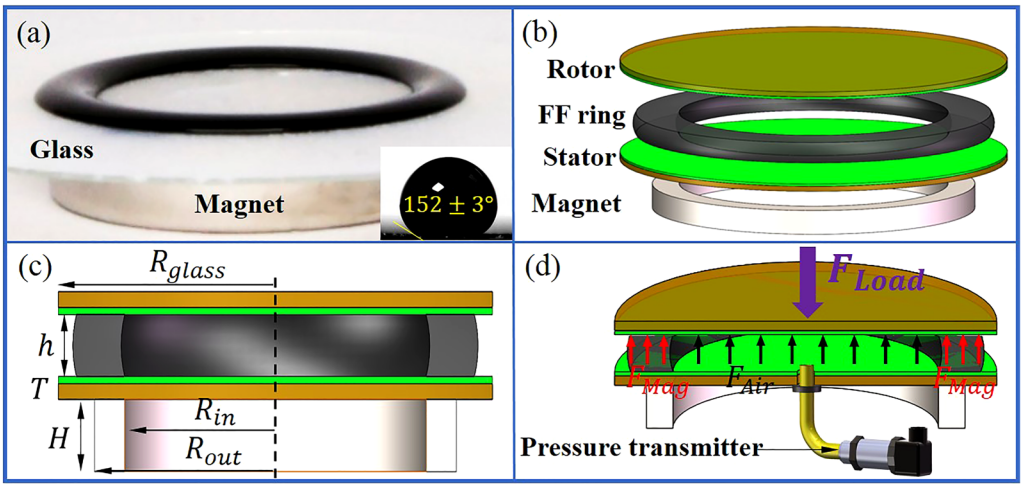

FIG. 1. (a) Image of FF located on a glass surface. (b) and (c) Construction of the bearing. (d) Sketch depicting the principles of support and testing of the bearing.

the liquid bridge bearing dominated by Laplace pressure, such magnetic pressure may work as a controllable supporting force to further improve the bearing capacity.

This study combines the merits of positioning and supporting features of the FF to propose a liquid bridge bearing that uses it as a liquid medium. A permanent magnet with an annular structure is constructed to locate the FF on a super-hydrophobic surface and form an FF ring. This liquid ring in conjunction with air sealed in the structure can provide the requisite carrying capacity. The theoretical model of the FF-lubricated bearing is established, and the calculated static supporting force is compared with that obtained through experiments. The repeatability and dynamic supporting force of the bearing are also discussed.

II. METHOD

Figure 1(a) shows the image of an FF located on a glass surface in the presence of a magnet ring. Figure 1(b) shows the construction of the FF-lubricated thrust bearing. It consists of a stator, a rotor, an FF ring, and a permanent magnet. The FF absorbed by the magnet persists in the gap between the glasses. The height of the gap is represented by h [Fig. 1(c)]. In this way, a certain volume of air is sealed by the FF ring to form an air cushion. As the rotor axial compresses, the FF as well as the air cushion can supply supporting forces. Figure 1(d) shows the principles of support and testing of the FF-lubricated thrust bearing.

A. Theoretical model of static supporting force

To determine the respective contributions of the FF (F_{Mag}) and the air cushion (F_{Air}) to the total supporting force, a model of the bearing, shown in Fig. 2(a), is studied theoretically. Compared with F_{Mag} and F_{Air}, the effects of Laplacian pressure and the capillary force are negligibly small.[14] Therefore, the total supporting force can approximately be regarded as the sum of F_{Mag} and F_{Air}.

Figure 2(b) presents the geometrical features of the model. Pressure inside the FF and the air cushion can be derived from the ferrohydrodynamic Navier–Stokes equations. For an incompressible Newtonian fluid, the pressure distribution inside the FF can be expressed as[15,16]

$$P_r - \mu_0 \int_0^{H_r} M_H dH = P_{r_{out}} - \mu_0 \int_0^{H_{r_{out}}} M_H dH, \tag{1}$$

where the pressure (P_r) inside the FF at a specific height (h) and radius (r) of the gap depends on the strengths of the magnetic field (H_r) and ($H_{r_{out}}$) and the atmospheric pressure ($P_{r_{out}}$). In addition, μ_0 is the permeability of free space and M_H is the magnetization of the FF.

Ignoring particle interactions, the magnetization (M_H) of a dilute FF is given by the Langevin function,[17]

$$M_H = M_s L(\alpha) = M_s \left(\frac{e^{2\alpha}+1}{e^{2\alpha}-1} - \frac{1}{\alpha} \right), \tag{2}$$

where M_s is the saturation magnetization of the FF and α is the Langevin parameter,

$$\alpha = \frac{\mu_0 m_d H}{kT}. \tag{3}$$

Here, m_d is the magnetic moment of the nanoparticle, H is the applied field, k is Boltzmann's constant, and T is the absolute temperature. By using the spontaneous magnetization of the magnetic material of the particles, one can rewrite their magnetic moment as

$$m_d = \frac{1}{6} M_d \pi d^3, \tag{4}$$

where $M_d = M_s/\emptyset_p$ is the spontaneous magnetization of solid particles, $\emptyset_p$ is the volume fraction of particles in the FF, and d is the

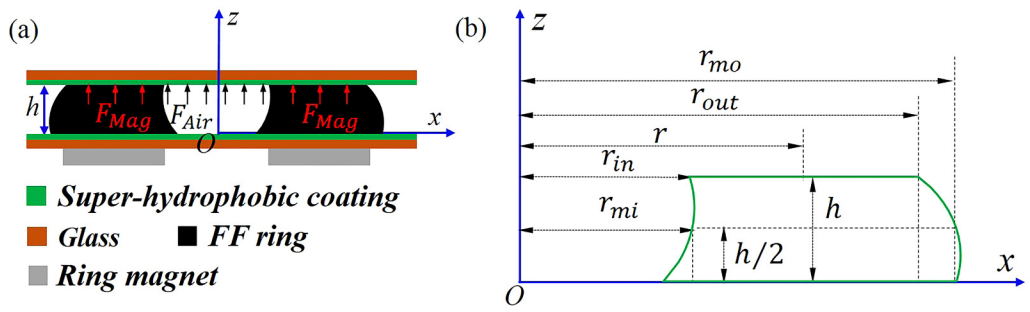

FIG. 2. (a) Cross-sectional image of the bearing. (b) Geometrical features for the cross-sectional view.

diameter of the magnetic nanoparticle. We define $K = \frac{\mu_0 m_d}{kT}$. Then, Eq. (1) can be rewritten as

$$\begin{aligned} P_r &= P_{r_{out}} + \mu_0 \int_{H_{r_{out}}}^{H_r} M_H dH \\ &= P_{r_{out}} + \mu_0 M_s \int_{H_{r_{out}}}^{H_r} \frac{e^{2KH}+1}{e^{2KH}-1} - \frac{1}{KH} dH \\ &= P_{r_{out}} + \mu_0 M_s \left(\int_{H_{r_{out}}}^{H_r} dH + \int_{H_{r_{out}}}^{H_r} \frac{2}{e^{2KH}-1} dH - \int_{H_{r_{out}}}^{H_r} \frac{1}{KH} dH \right) \\ &= P_{r_{out}} + \mu_0 M_s \left[\frac{1}{K} \left(\ln \frac{e^{2KH_r}-1}{e^{2KH_{r_{out}}}-1} - \ln \frac{H_r}{H_{r_{out}}} \right) - (H_r - H_{r_{out}}) \right]. \end{aligned} \tag{5}$$

Therefore, the supporting force of the magnetized FF (F_{Mag}) can be obtained by integrating the area element of the pressure difference between P_r and $P_{r_{out}}$. This can be written as

$$\begin{aligned} F_{Mag} &= \int_{r_{in}}^{r_{out}} P_r - P_{r_{out}} dA \\ &= 2\pi\mu_0 M_s \int_{r_{in}}^{r_{out}} \left[\frac{1}{K} \left(\ln \frac{e^{2KH_r}-1}{e^{2KH_{r_{out}}}-1} - \ln \frac{H_r}{H_{r_{out}}} \right) - (H_r - H_{r_{out}}) r dr \right]. \end{aligned} \tag{6}$$

The pressure in the air cushion (P_{Air}) can be written as

$$\begin{aligned} P_{Air} &= P_{r_{in}} - P_{r_{out}} \\ &= \mu_0 M_s \left[\frac{1}{K} \left(\ln \frac{e^{2KH_{r_{in}}}-1}{e^{2KH_{r_{out}}}-1} - \ln \frac{H_{r_{in}}}{H_{r_{out}}} \right) - (H_{r_{in}} - H_{r_{out}}) \right]. \end{aligned} \tag{7}$$

The supporting force of the air cushion (F_{Air}) may be obtained by integrating P_{Air} over the air supporting region,

$$\begin{aligned} F_{Air} &= \pi r_{in}^2 P_{Air} \\ &= \pi r_{in}^2 \mu_0 M_s \left[\frac{1}{K} \left(\ln \frac{e^{2KH_{r_{in}}}-1}{e^{2KH_{r_{out}}}-1} - \ln \frac{H_{r_{in}}}{H_{r_{out}}} \right) - (H_{r_{in}} - H_{r_{out}}) \right]. \end{aligned} \tag{8}$$

Therefore, the total supporting force can be rearranged as

$$\begin{aligned} F_{Supporting} &= F_{Mag} + F_{air} \\ &= 2\pi\mu_0 M_s \int_{r_{in}}^{r_{out}} \left[\frac{1}{K} \left(\ln \frac{e^{2KH_r}-1}{e^{2KH_{r_{out}}}-1} - \ln \frac{H_r}{H_{r_{out}}} \right) - (H_r - H_{r_{out}}) \right] r dr \\ &\quad + \pi r_{in}^2 \mu_0 M_s \left[\frac{1}{K} \left(\ln \frac{e^{2KH_{r_{in}}}-1}{e^{2KH_{r_{out}}}-1} - \ln \frac{H_{r_{in}}}{H_{r_{out}}} \right) - (H_{r_{in}} - H_{r_{out}}) \right]. \end{aligned} \tag{9}$$

To calculate the total supporting force ($F_{Supporting}$), the key is to determine the positions of r_{in} and r_{out} as well as the corresponding strengths of the field. Because the morphological characteristic of the border of the FF is decided by the spatial distribution of the magnetic field of the annular magnet, the problem can be addressed numerically by a finite element simulation of the magnetic field. The input magnetic and geometrical parameters are consistent with the applied magnetic field. Figure 3 shows curves of the typical distribution of the field strength over the radial direction of the magnet at two heights. When the rotor is at a specific height (e.g., $h = 0.6$ mm), the inner interface of the FF at this height should remain at the position where the magnetic field strength $H_{r_{in}}$ is the largest along the radial direction.[15] Therefore, the specific data of r_{in} can be obtained based on the curve of distribution of the field at a certain height.

The next task is to determine the position of r_{out}. Because the inner and outer interfaces of the FF are curved, the cross-sectional image shown in Fig. 2(b) can be regarded approximately as a rectangle to improve the accuracy of calculation. Then, at a height $h/2$, the corresponding radii of the inner and outer interface of the FF are defined as r_{mi} and r_{mo}, respectively. As shown in Fig. 2(a), the pressure in the cushion acting on the inner interface of the FF is equal everywhere, which means that the inner interface is subjected to the equivalent strength of the magnetic field at different heights. Then, $H_{r_{in}} = H_{r_{mi}}$. Therefore, the value of r_{mi} can be obtained based on the curve of distribution of the magnetic field at height $h/2$. As shown in Fig. 3, at height $h/2$ (e.g., $h/2 = 0.3$ mm), the magnetic strength of the two points (r_{mi} and r'_{mi}) is equal to $H_{r_{in}}$. Because air pressure in the sealed chamber is not sufficiently high to pass though the magnetic pressure difference at this height, only r_{mi}

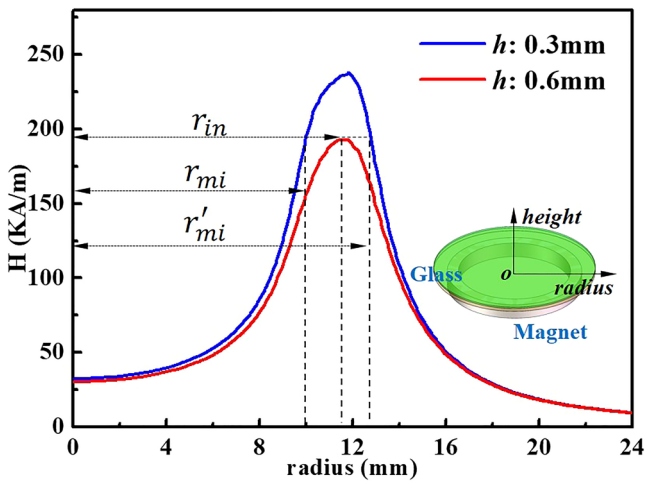

FIG. 3. Distribution of magnetic field strength at two heights above the lower glass.

meets the condition. We can thus obtain r_{mi}. Because the FF is incompressible, its volume can be roughly calculated as

$$V \approx \pi(r_{mo}^2 - r_{mi}^2)h. \tag{10}$$

Thus, the value of r_{mo} at a height of $h/2$ can be obtained, and the corresponding magnetic field strength ($H_{r_{mo}}$) can be calculated based on the curve of distribution of the magnetic field because the magnetic field strength applied on the outer interface of the FF is equal everywhere, namely, $H_{r_{mo}} = H_{r_{out}}$. Similarly, $H_{r_{out}}$ can be determined according to the curve of distribution of the magnetic field at height h. Then, the position of r_{out} at h can be determined.

B. Experimental measurement of supporting force

The supporting force of the bearing was predicted using theoretical calculations presented above and measured using a force-testing platform. Figure 1(d) shows the schematic diagram of the testing principle. Instead of the traditional water bridge bearing, a water-based FF was chosen for the measurement, and its parameters are given in Table I. Glasses of size $\Phi 50 \times 0.5\ mm^2$ were used as the stator and the rotor of the thrust bearing. To reduce the loss of the FF, the working surfaces of the bearing were coated with a super-hydrophobic paint (Never Wet, Ross Technology Corp., USA),[18] and the contact angle of the FF on the coated glass was about $\sim 152 \pm 3°$. The axial magnetic field was supplied by an annulus magnet (Maximum Energy Product 35 MGOe, NdFeB) of size $\Phi 25 \times 20 \times 5\ mm^3$.

Before the experiment, 0.2 ml of FF was dropped on the surface of the stator to form the FF ring. The rotor connected to a tension–compression sensor then moved in the axial direction at a speed of 0.008 mm/s. The range of measurement and resolution of the force sensor were 5 and 0.001 N, respectively. As the rotor pressed down, the data of the supporting force were recorded. A pressure transmitter was linked to the hole of the lower glass. The evolution of pressure in the cushion was also recorded during compression. The static and dynamic supporting forces were defined as the rotor shifting down without and with rotation, respectively. In addition, multicycle loading/unloading experiments were carried out to test the repeatability of the supporting forces.

TABLE I. Main properties of ferrofluid.

Parameters	Value
Nanoparticles	Fe_3O_4
Particle diameter, d	10 ± 2 nm
Volume fraction of nanoparticles, $\emptyset_p$	4.3%
Density, ρ	1.2 g/cm^3
Dynamic viscosity, η	5 mPa s
Surface tension, γ	32 mN/m
Saturation magnetization, M_s	1.52×10^4 A/m

III. RESULTS AND DISCUSSION

Figure 4 presents both the experimental and the theoretical results of the static supporting force of the bearing as a function of the height of the gap (h). The experimental total force increased as the rotor moved down. When the height of the gap between the rotor and the stator was 0.25 mm, the total force was 3.2 N, far greater than that due to a liquid bridge bearing dominated by Laplace pressure.[9] Compared with the traditional liquid bearing, the curve of the force of the FF bearing was stable during compression and exhibited no fluctuation. In the traditional liquid bridge bearing, a drop of water may escape from the liquid ring when the contact angle of the liquid approaches the value of the advancing contact angle on the hydrophobic surface.[19] As a result, the supporting force

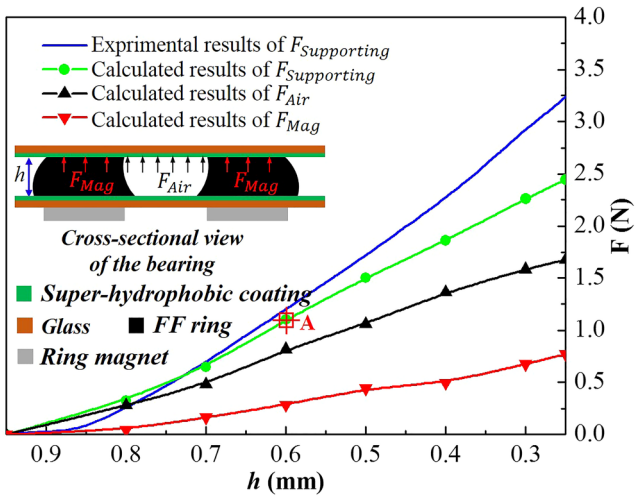

FIG. 4. Comparison of the experimental and theoretical values of the static supporting force of the bearing.

may suddenly decrease. However, in the proposed FF bearing, due to the presence of the magnetic field, the FF was anchored to the surface of the stator and suffered no loss in supporting force. Therefore, using the FF as liquid medium for the bearing not only increased the supporting capacity but also improved the stability of the support.

Based on Eq. (9), the total theoretical bearing capacity, which consists of F_{Mag} and F_{Air}, was calculated. The theoretical values of F_{Mag} and F_{Air} both increased with decreasing gap height (h) between the rotor and the stator. Both the experimental and the theoretical values of total force increased with decreasing gap height. A deviation between the experimental and theoretical values might have been obtained from two sources. One was air leakage, which will be discussed in the section of quantifing the contribution of the air cushion. The other is that the Laplacian pressure of the FF was not included in the calculations of the model. As the indenter shifted down, the radius of curvature of the FF–gas interface decreased, which might have increased the Laplacian pressure. Thus, the deviation between the experimental and the theoretical values increased with decreasing gap height.

We now provide an example of the calculation at a gap height of 0.6 mm. As shown in Fig. 3, the inner radius of the interface of the FF $r_{in} = 11.4$ mm can be obtained from the curve of distribution of the magnetic field. The magnetic field strength at this point was $H_{r_{in}} = 192.6$ KA/m. Due to the equivalent field strength at r_{in} and r_{mi}, the value of $r_{mi} = 9.96$ mm was obtained at a height of $h/2$ (gap height: 0.3 mm). According to Eq. (10), $r_{mo} = 14.33$ mm. So the value of $H_{r_{mo}} = 94.83$ KA/m was obtained from the curve of distribution of the magnetic field at a height of $h/2$ (0.3 mm). Because $H_{r_{mo}} = H_{out}$, $r_{out} = 14.13$ mm was derived from the curve of distribution of the field at a gap height of h (0.6 mm). Subsequently, $F_{Mag} = 0.286$ N and $F_{air} = 0.817$ N were obtained according to Eqs. (6) and (8), respectively. Hence, the calculated force of the bearing was about 1.103 N (point A in Fig. 4), close to the experimental value of 1.198 N.

In Fig. 4, the calculated F_{air} is consistently higher than F_{Mag} over a range of gap heights. To confirm the role of the air cushion, the total forces of the FF bearing with and without the sealed air cavity were measured and compared. As shown in Fig. 5, for the sample with the bottom unsealed (without air cushion), an air vent opened on the lower stator. In this way, the internal and external pressures of the FF ring were the same, and bearing capacity was supplied only by the magnetized FF ring. For the sample with the bottom sealed (with air cushion), the total supporting force was shared by the FF and air. The experimental results show that the force of the FF-only support was far smaller than that of the FF bearing with the air cushion. It thus seems that the participation of the air cushion significantly increased the total supporting capacity.

To further quantify the contribution of the air cushion of the FF bearing, experiments were performed to monitor the variation in the pressure in it during compression. Figure 6 shows the results of three groups of independent experiments. The curves of pressure showed almost the same tendency, indicating good repeatability. The maximum pressure reached 5.3 KPa when the gap height between the rotor and the stator was 0.25 mm. Based on Eq. (7), the theoretical pressures in the air cushion were also calculated at different gap heights. The deviation between the theoretical and experimental results can be attributed to air leakage. During

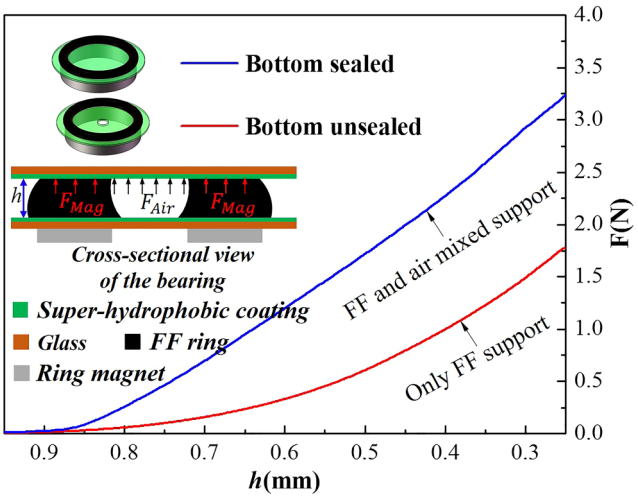

FIG. 5. Experimental comparison of the static supporting forces of the FF bearing with and without the air cushion.

compression, as the air pressure was higher than the seal capability of the FF, some of the air in the FF-sealed chamber escaped. The experimental result was transient such that the air leakage was not complete. However, the value obtained by the model was based on the sealing capability of the FF, and the result reflected a steady state. This means that air had leaked out completely, causing the calculated air pressure to be lower than that measured experimentally.

To explore the repeatability of the static supporting force, four load–retract cycles were performed, and the results are shown in Fig. 7. For the first loading and unloading period, the interval of

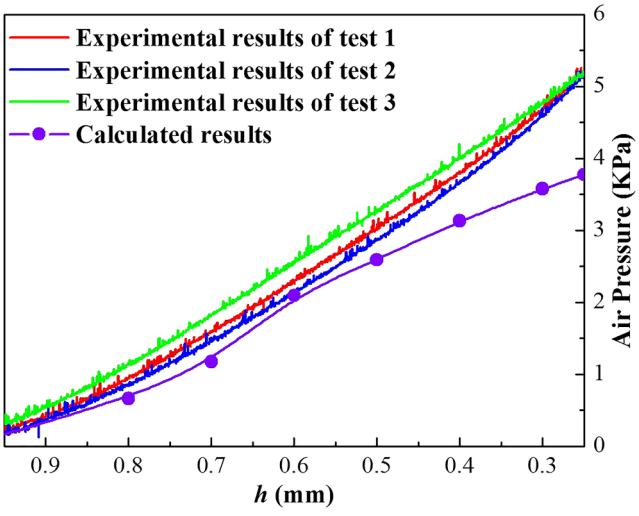

FIG. 6. Comparison of the experimental and theoretical values of pressure in the air cushion.

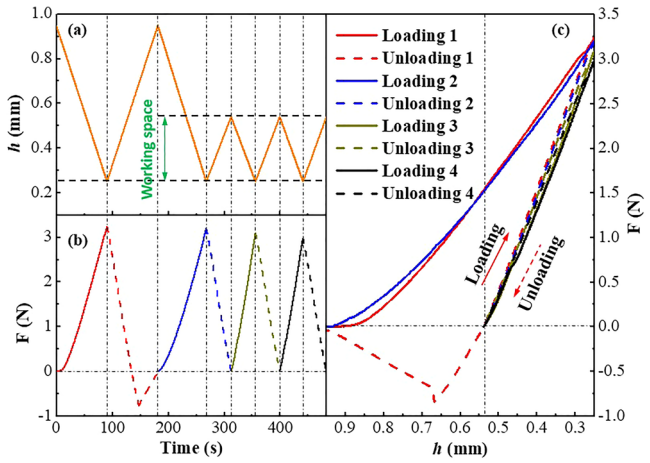

FIG. 7. Multiple load–retract cycles of the FF bearing. (a) Range of displacement of the rotor. (b) Range of force of the FF bearing. (c) Repeated accuracy of the static supporting force.

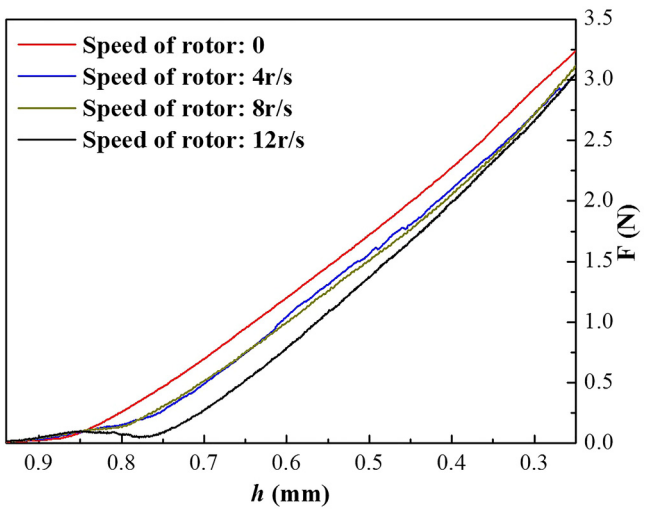

FIG. 8. Effect of speed of the rotor on the supporting force of the FF bearing.

displacement of the gap was 0.95–0.25 mm [Fig. 7(a)]. When the height of the gap was reduced to 0.25 mm, the total static supporting force was 3.2 N. During the unloading process, zero force appeared not at a gap height of 0.95 mm but at about 0.54 mm. As the rotor continued to move up, negative force was detected and continued to grow. Because F_{Mag} was positive, the negative supporting force means that the pressure of the air cushion was lower than atmospheric pressure. Such a phenomenon indicates that the air had leaked during loading. The maximal force was −0.75 N as the rotor moved up to a height of 0.66 mm. When the rotor went back continually to its original height of 0.95 mm, the negative force gradually decreased to zero again. In this process, the value of F_{Mag} decreased owing to the declining strength of the magnetic field. However, the value of the negative supporting force decreased as well, which means the outer air flowed across the FF ring and returned to the chamber. The hysteresis of the loading/unloading was due to the expulsion of air during loading and its intake during unloading. It seems that to attain the repeatability of the supporting force during the load–retract process, the rotor should be shifted at appropriate intervals in which no air leaks into or out of the FF ring.

For the remaining three load–retract cycles, the displacement of the rotor was in the range of 0.54–0.25 mm. As is shown in Fig. 7(c), the curves of force during loading and unloading exhibited good repeatability in this range of the gap. This shows that no air leaked through the FF-sealed chamber during the loading/unloading process within this range of displacement. Therefore, according to the first load–retract cycle, a reasonable working space (e.g., 0.54–0.25 mm) of the FF bearing can be obtained, in which the supporting force of the bearing has repeatable accuracy. In general, during the first unloading process, the gap height, where the first zero support force appeared (corresponding to 0.54 mm), might be defined as the maximum height of the rotor. Hence, a bearing working in the range between the minimum and maximum gap heights can achieve remarkable and repeated accuracy. The working space is variable and is based on the minimum gap height for the first cycle.

In applications, the bearing always works in dynamic conditions. Is the theoretical calculation here suitable for predicting the dynamic supporting force?

Figure 8 presents the dynamic supporting force of the FF bearing at four rotational speeds (0, 4, 8, and 12 r/s). The dynamic supporting forces were slightly lower than the static force in general. In addition, the rotational speed had a weak effect on the dynamic supporting force. The lower the gap height was, the smaller was the difference in force. Such behaviors are significantly different from that of the traditional liquid bridge bearing.[9] Due to the existence of the magnetic field, the dipole of each magnetic particle tends to align in the direction of the field.[20] This response may obstruct the movement of the suspended particles as well as the flow behaviors of the FF. The most immediate consequence is no escape from the FF because the effect of centrifugal force on it is inhibited. Moreover, a strong magnetoviscous effect[21] may restrain the laminar velocity of the FF during the shear motion of the rotor. Therefore, Eq. (9) might also be applied to estimate the dynamic supporting force of the bearing with low requirements.

From the viewpoint of application, friction tests were carried out to verify the supporting capacity of the bearing. Figure 9 shows the friction curves of the FF-lubricated thrust bearings with and without the magnet. The bearing sample with the magnet was the same as in Fig. 4. A normal load of 2 N was applied, lower than the total supporting capacity of the bearing (Fig. 4). The tribo-pairs were isolated by the air cushion and the FF together, and the friction force merely came from the viscous force of the FF. Therefore, its coefficient of friction was very low. For the bearing without the magnet, a majority of the FF between the tribo-pairs was squeezed out under the normal load, and local asperity contact occurred. The friction coefficient was much higher than that of the FF-lubricated thrust bearing with the magnet.

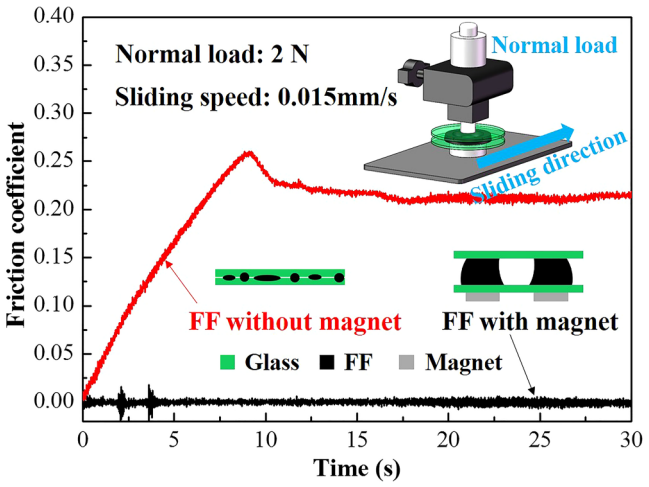

FIG. 9. Friction curves of the FF-lubricated thrust bearing with and without the magnet (the bearing sample used was the same as that shown in Fig. 4).

IV. CONCLUSIONS

This study examined the static/dynamic supporting force of an FF-lubricated thrust bearing with an air cushion. The magnetic pressure of the magnetized FF was used to generate the liquid support (F_{Mag}), and air support (F_{Air}) was supplied by the gas sealed in the FF ring. A theoretical model of the FF bearing was used to calculate F_{Mag} and F_{Air}. Experiments were also performed to measure the supporting forces with and without rotation. The results showed that the theoretical model can approximately predict the load capacity of the nonrotating bearing. Compared with the FF support, the air cushion contributed to more than half of the total force. Multicycle load/unload results exhibited hysteresis and indicated that force values with good and repeated accuracy were obtained only within a limited range of oscillation in gap height. Moreover, when the bearing was rotating, the load capacity was nearly independent of the rate of rotation. The proposed model reasonably approximated the empirical bearing capacity under conditions that approximated the fixed boundary conditions for the shape of the free FF surface.

SUPPLEMENTARY MATERIAL

See the supplementary material for the complete process of the calculation of F_{Mag}, F_{Air}, $F_{Supporting}$, and P_{Air}.

ACKNOWLEDGMENTS

This work was supported by the National Natural Science Foundation of China (No. 51875278) and the National Key Laboratory of Science and Technology on Helicopter Transmission (No. HTL-A-20G03). The authors have no conflicts to disclose.

DATA AVAILABILITY

The data that support the findings of this study are available within the article and its supplementary material.

REFERENCES

[1]S. Boyde, R. Soc. Chem. **4**, 293 (2002).
[2]E. Andablo-Reyes, J. de Vicente, R. Hidalgo-Álvarez, C. Myant, T. Reddyhoff, and H. A. Spikes, Tribol. Lett. **39**, 109–114 (2010).
[3]G. Sun, T. Liu, P. Sen, W. Shen, C. Gudeman, and C.-J. Kim, J. Microelectromech. Syst. **23**, 147–156 (2014).
[4]M. L. Chan, B. Yoxall, H. Park, Z. Kang, I. Izyumin, J. Chou, M. M. Megens, M. C. Wu, B. E. Boser, and D. A. Horsley, in *IEEE 24th International Conference on Micro Electro Mechanical Systems* (IEEE, 2011), p. 1237.
[5]M. Mastrangeli, Adv. Mater. **27**, 4254–4272 (2015).
[6]M. L. Chan, B. Yoxall, H. Park, Z. Kang, I. Izyumin, J. Chou, M. M. Megens, M. C. Wu, B. E. Boser, and D. A. Horsley, Sens. Actuators A Phys. **177**, 1–9 (2012).
[7]B. E. Yoxall, M.-L. Chan, R. S. Harake, T. Pan, and D. A. Horsley, J. Microelectromech. Syst. **21**, 721–729 (2012).
[8]T. Gillespie, J. Colloid Interface Sci. **36**, 119–123 (1971).
[9]J. Wen, D. Dini, and T. Reddyhoff, Tribol. Int. **149**, 8 (2020).
[10]S. Odenbach, Colloids Surf. A **217**, 171–178 (2003).
[11]Y. Melikhov, S. J. Lee, D. C. Jiles, D. H. Schmidt, M. D. Porter, and R. Shinar, J. Appl. Phys. **93**, 8438–8440 (2003).
[12]W. Huang, C. Shen, S. Liao, and X. Wang, Tribol. Lett. **41**, 145–151 (2011).
[13]C. M. Oldenburg, S. E. Borglin, and G. J. Moridis, Trans. Porous Media **38**, 319–344 (2000).
[14]X. Xie, Q. Dai, W. Huang, and X. Wang, J. Phys. D: Appl. Phys. **54**, 175004 (2021).
[15]S. Lampaert, J. W. Spronck, and R. Ostayen, Proc. Inst. Mech. Eng. Part J J. Eng. Tribol. **232**, 14–25 (2018).
[16]Z. H. Wei and C. P. Lee, J. Appl. Phys. **105**, 07B523 (2009).
[17]L. Vékás, M. Rașa, and D. Bica, J. Colloid Interface Sci. **231**, 247–254 (2000).
[18]H. B. Hu, J. Wen, L. Y. Bao, L. B. Jia, D. Song, B. W. Song, G. Pan, M. Scaraggi, D. Dini, Q. J. Xue, and F. Zhou, Sci. Adv. **3**, 1–9 (2017).
[19]J. Wen, T. Reddyhoff, S. T. Hu, D. Puhan, and D. Dini, Tribol. Int. **144**, 106129 (2020).
[20]A. N. Afifah, S. Syahrullail, and N. A. C. Sidik, Renew. Sustainable Energy Rev. **55**, 1030–1040 (2016).
[21]C. Holm and J. Weis, Curr. Opin. Colloid Interface Sci. **10**, 133–140 (2005).